atmosphere

MDPI

Article

Ship-Borne Observations of Atmospheric CH_4 and $\delta^{13}C$ Isotope Signature in Methane over Arctic Seas in Summer and Autumn 2021

Natalia Pankratova [1,*], Andrey Skorokhod [1], Igor Belikov [1], Valery Belousov [1], Valeria Muravya [2] and Mikhail Flint [2]

[1] A.M. Obukhov Institute of Atmospheric Physics, Russian Academy of Sciences, 119017 Moscow, Russia; askorokhod@mail.ru (A.S.); belikov@ifaran.ru (I.B.); belousov@ifaran.ru (V.B.)
[2] Shirshov Institute of Oceanology, Russian Academy of Sciences, 117997 Moscow, Russia; muravya.vo@ocean.ru (V.M.); m_flint@ocean.ru (M.F.)
* Correspondence: pankratova@ifaran.ru

Abstract: Determining the sources of methane emissions in the Arctic remains a complex problem, due to their heterogeneity and diversity. Information on the amount of emissions has significant uncertainties and may differ by an order of magnitude in various literature sources. Measurements made in the immediate vicinity of emission sources help to clarify emissions and reduce these uncertainties. This paper analyzes the data of three expeditions, carried out in the western Arctic seas during Arctic spring, summer, and early autumn in 2021, which obtained continuous data on the concentration of methane and its isotope signature $\delta^{13}C$. CH_4 concentrations and $\delta^{13}C$ displayed temporal and spatial variations ranging from 1.952 to 2.694 ppm and from −54.7‰ to −40.9‰, respectively. A clear correlation was revealed between the surface methane concentration and the direction of air flow during the measurement period. At the same time, even with advection from areas with a significant anthropogenic burden or from locations of natural gas mining and transportation, we cannot identify particular source of emissions; there is a dilution or mixing of gas from different sources. Our results indicate footprints of methane sources from wetlands, freshwater sources, shelf sediments, and even hydrates.

Keywords: arctic methane; methane emissions; stable isotopes

Citation: Pankratova, N.; Skorokhod, A.; Belikov, I.; Belousov, V.; Muravya, V.; Flint, M. Ship-Borne Observations of Atmospheric CH_4 and $\delta^{13}C$ Isotope Signature in Methane over Arctic Seas in Summer and Autumn 2021. *Atmosphere* **2022**, *13*, 458. https://doi.org/10.3390/atmos13030458

Academic Editors: John Walsh, Uma S. Bhatt and Muyin Wang

Received: 30 December 2021
Accepted: 8 March 2022
Published: 11 March 2022

1. Introduction

Significant reserves of methane are concentrated in the Arctic region, including the water column and seabed; however, some of the marine sources are poorly investigated. For example, various estimates of methane emissions from the sea surface at high latitudes differ by more than three orders of magnitude: from 0.013 to 20 Tg yr^{-1} [1–8]. Methane can enter the ocean from several sources, such as biogenic production in oxic surface waters, the formation of methane in bottom sediments, thermogenic (fossil) methane, and lateral transport by rivers. As a rule, it is difficult to separate the contribution from any of the listed sources due to the complexity of measurements. Even with the involvement of data on the isotopic signature of methane $\delta^{13}C$ in the ambient air, the results show the presence of mixed sources [9–11].

In addition, there is no unified conception of which region makes the greatest contribution to Arctic marine emissions. Thus, in [4,5,12], it was concluded that the East Siberian Arctic Shelf (ESAS) gives from 10 to 17 Tg yr^{-1} on the basis of data from a number of marine expeditions. ESAS is the widest and shallowest shelf of the World Ocean and contains considerable reserves of submarine permafrost [13]. Methane hydrate stability is maintained in the special thermobaric conditions; the source hydrates, according to some estimates, may exceed by two orders of magnitude the total amount of methane in the

atmosphere. As estimated in [4,5,10], it is implied that the main reason for such significant emissions is gas releasing from seabed associated with the destabilization of methane hydrates. At the same time, estimates presented in [14–17] evaluate emissions from ESAS as insignificant. In [3], the contribution of methane hydrates to atmospheric emissions was estimated at <0.1 Tg yr^{-1}. In other works, such as Thornton et al., 2020 and Yurganov et al., 2016, ESAS annual flux was estimated as ~3 Tg yr^{-1} and ~6 Tg yr^{-1}, respectively [8,18].

At the same time, analysis of satellite data shows a rather significant contribution of marine emissions in the Western Arctic during late autumn and winter periods [6]. Yurganov et al. (2021) tentatively estimated its annual value as ~2/3 of the Earth's methane emissions north of 60° N. While the most common estimates of emissions from terrestrial ecosystems north of 60° N are in the range of 20 to 30 Tg yr^{-1} [3,19] (according to [20], 3–4 times more), the contribution from oceanic emissions at a minimal estimate can be in the range 15–20 Tg yr^{-1}, representing 3–4% of global emissions. The amplitude of the seasonal atmospheric CH_4 cycle increases in many areas but is especially noticeable in the Kara and Barents Seas (40–50% of the Arctic marine emissions) [6]. At the same time, the methane flux throughout the ocean surface is insignificant during the warm period, which is consistent with the data of [21]. Such seasonal differences, apparently, are associated with an increase in wind speed in winter, an increase in the number of stormy days, reducing of ice cover, and, as a consequence, a breakdown of water column stratification. Despite such a wide range of estimates of methane emissions, several studies indicate an increase in emissions during ongoing climate change [12,22–25].

Sources of methane. The main sources of CH_4 in the Arctic are natural wetlands, inland water bodies (lakes, streams, deltas, estuaries), leaks from oil and gas production and transportation, wildfires, emissions from the seabed, and geological seepage. The total contribution from boreal and tundra biomes (for latitudes > 50° N) is estimated to be approximately 25 to 100 Tg yr^{-1} [26], while share of emissions from wetlands continues to increase due to climate change and permafrost thawing. For example, methane emissions from arctic wetlands (>67° N) increased by 30.6 ± 0.9% in the period from 2003 to 2007 [27].

Analysis of data of the isotopic signature $\delta^{13}C$ in methane [28–32] is necessary information in this case. The ^{13}C:^{12}C ($\delta^{13}C$) ratio in CH_4 is used to identify the sources of methane. Light CH_4 (depleted in ^{13}C) is emitted mainly during biological production and varies markedly depending on the oxidation state (for example, during transport in soil or water). Heavy CH_4 (relatively enriched in ^{13}C compared to biological sources) generally comes from pyrogenic and thermogenic sources such as biomass combustion and coal mines. However, wide temporal and geographical variations in the isotope signature are often observed for each category. So, for example, the $\delta^{13}C$ value can vary from −60 to −78‰ for the wetlands of Finland, depending on the season, with the highest frequency being −68–74‰ [33]. Methane hydrates correspond to $\delta^{13}C$ equal to −55‰ [34]; wildfires give −26‰ [35]; and gas leakages correspond to −42‰ [36,37]. Figure 1 shows typical variations in $\delta^{13}C$ for various sources of CH_4, while other literature sources may differ by several units from those presented here. In addition, many sources have similar signatures, which greatly complicates the assessment of source determination of the observed methane emissions. Thus, it is necessary to measure methane and its isotope signature $\delta^{13}C$ in the immediate vicinity of the sources for a more reliable identification of sources. Oceanographic campaigns are one such instrument. The main goal is investigation of the features of the distribution of methane emissions in the Arctic (e.g., [9,12,17,38–40]).

This paper presents the results of ship-borne measurements of methane and its isotope signature performed in the Norwegian, Barents, Kara, and White Seas in 2021. One cruise was made for Arctic spring; the Kara Sea was partly covered by ice. Two other cruises were made during the navigation period when the seas were free of ice, i.e., according to [6], emissions in the ocean-atmosphere system were insignificant. Thus, the large-scale advection of air masses can be considered as the main factor of the variability of the surface methane concentration over the sea. The results of this research may be of interest in terms

of studying regional transport of air masses and its influence on the dynamics of methane in the Arctic region.

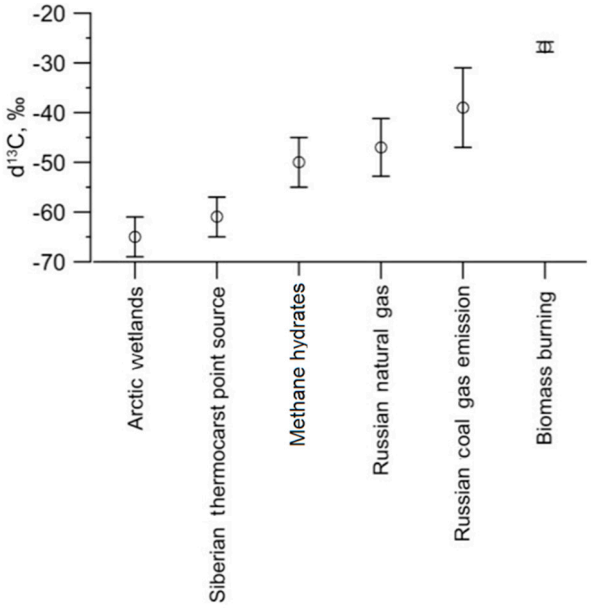

Figure 1. Range of $\delta^{13}C$ in CH_4 for different sources according to [41] France et al. (2016).

2. Materials and Methods

An automated analysis system [9,10] based on the G2132-i instrument manufactured by Picarro Inc. (USA, Santa Clara, California) was used for obtaining the data analyzed in this paper. This instrument is designed to measure methane mole fraction in the range of 1800 to 12,000 ppb with a precision of less than 5 ppb and to measure the $\delta^{13}C_{CH4}$ value with a precision of less than 0.8‰. The time resolution of the instrument is about 30 s, according to the manufacturer's data sheet. Such a property will not affect the average concentration picture, with averaging of 10 min or more in any case [9].

The instrument was calibrated as follows. First, it was previously calibrated according to a secondary standard, which was a 1 L cylinder with compressed air provided by the NILU (Norwegian Institute for Air Research, Kjeller, Norway) with definite methane, CO_2, and $\delta^{13}C$ values, calibrated, in turn, to known international standards [8]. Then, the instrument calibrated thus was used to measure the true concentrations in cylinders with calibration gas mixtures (CGMs) provided by Linde Gas Rus company (Moscow region, Russia) with a significantly better accuracy than the CGMs themselves. Subsequently, this allowed the use of these CGMs as secondary standards as well as the checking of the long-term stability of the instrument readings. Calibrations were carried out before and after each expedition.

The analysis system was located in a cabin at the deck of the research vessel steering bridge. The air inlet was a downward funnel fixed at open air (see Figure 2) at 18.5 m height above sea level with PTFE tubing 1/8″ OD and 10 m length. Air flow was maintained at 1.5 L/min with a special pump of the complex, and the transit time from the inlet to the instrument turned out to be about 3 s.

Continuous observations of CH_4 mole fraction, carbon dioxide, and water vapor concentrations, as well as the values of the isotopic signature $\delta^{13}C$ in methane, were carried out in the ambient air of the seas of the Arctic region in the periods of 19 June to 5 July, 29 July to 25 August, and 27 August to 29 September 2021 from the board of the research vessel (R/V) Akademik Mstislav Keldysh (cruisers AMK-83, AMK-84, and AMK-85). The path of the AMK-83 ran from the port of Arkhangelsk, Russia through the White and Barents Seas to the Kara Sea, in which observations were made in the areas of the St. Anna Trough and the Novaya Zemlya archipelago; the final destination of the cruise was the

port of Arkhangelsk. The path of the AMK-84 cruise ran from the port of Arkhangelsk to the Barents Sea and the Norwegian-Greenland basin to the Spitsbergen archipelago, then through the Fram Strait to the southwestern periphery of the Nansen Basin and then through the Barents Sea to the port of Arkhangelsk. The route of the AMK-85 cruise ran from the port of Arkhangelsk through the White and Barents Seas to the Kara Sea, where observations were made in the areas of the Novaya Zemlya islands and the Novaya Zemlya depression and then to the port of Arkhangelsk. Route maps of the AMK-83, AMK-84, and AMK-85 cruises and the distribution of methane mole fraction in the surface layer along the expedition route are shown in Figure 3.

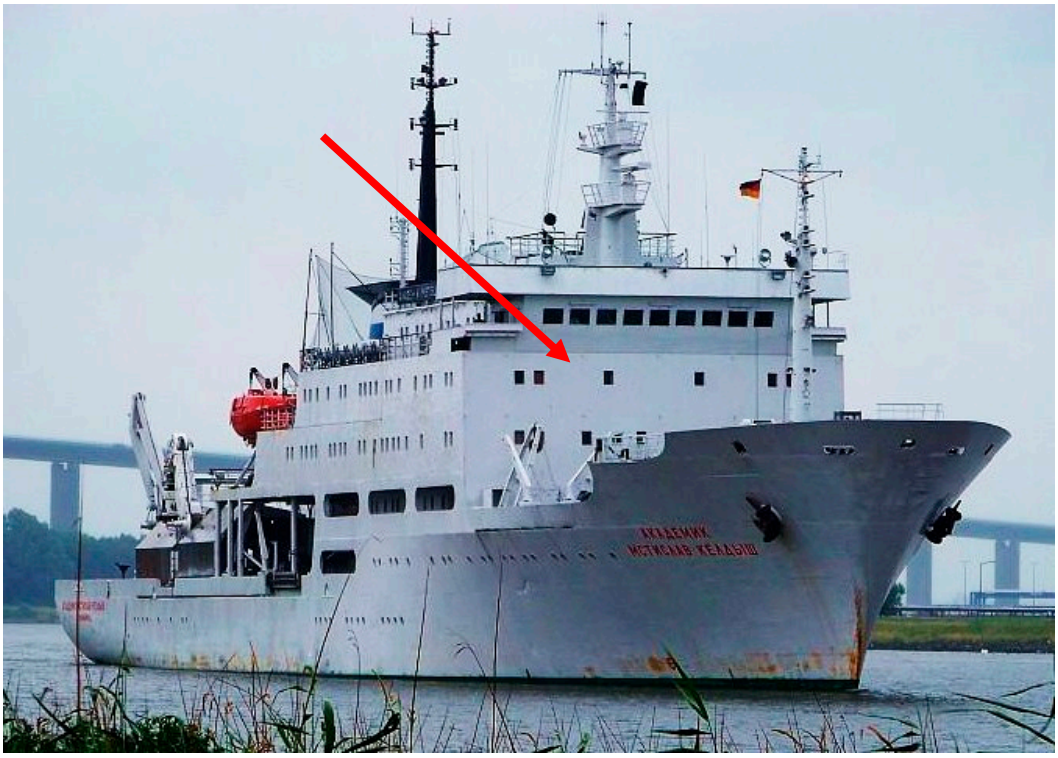

Figure 2. Location of the analysis system air inlet (indicated by red arrow) aboard the R/V Akademik Mstislav Keldysh. 18.5 m—measurement height above sea level.

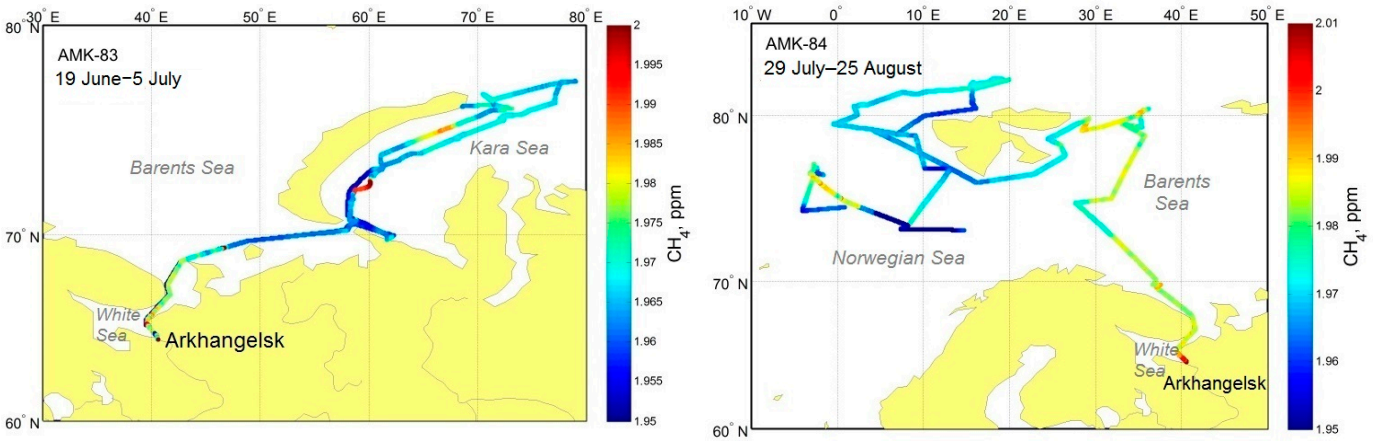

(**a**) (**b**)

Figure 3. *Cont.*

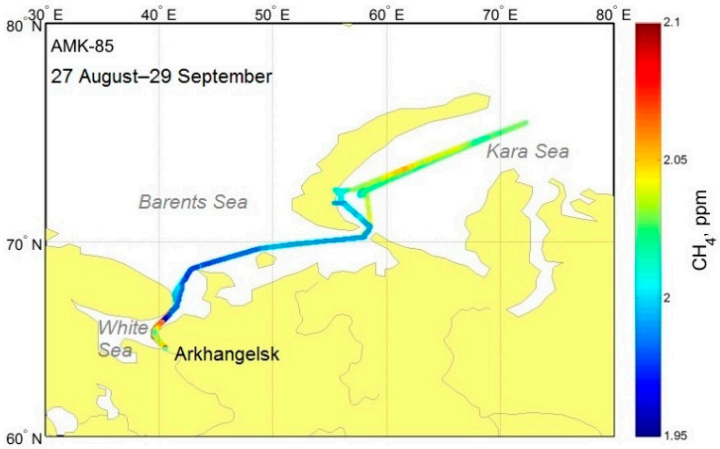

(**c**)

Figure 3. Variation in methane mole fraction in surface layer during the cruises of R/V Akademik Mstislav Keldys in summer and autumn of 2021 (AMK-83 (**a**), AMK-84 (**b**), and AMK-85 (**c**)).

Data filtering. Data from a meteorological station (AIRMAR 150WX, (AIRMAR Technology Corp., Milford, NH, USA) was used to exclude the influence of the ship's stack emissions. We used the relative wind direction, where a tailwind could bring smoke from the ship's chimney back onto the system and thus contaminate the measurements. We also used CO_2 data; potentially contaminated data corresponded to an increase in concentration of 10 ppm or more from the mean for each analyzed region. In total, about 7% of the data were flagged as potentially contaminated by the ship and not considered in the following analysis.

3. Results

Separate regions were allocated for three expeditions: White Sea, Barents Sea, Kara Sea, Norwegian Sea, and for the port of Arkhangelsk. The statistical characteristics were calculated for these areas and for the concentration of CH_4 and isotopic signature $\delta^{13}C$ (Table 1). The obtained dataset allows us to identify some regularities in the spatial and temporal variability of the methane concentration in the lower atmosphere; first of all, there is a good correspondence between the CH_4 concentration values and the direction of air mass removal in the periods of analyzed cruises.

Table 1. 1-minute averaged data from sea expeditions of the R/V Akademik Mstislav Keldysh in 2021; $\delta^{13}C$ (‰), CH_4 (ppm).

19 June–5 July AMK-83	Port		White Sea		Barents Sea		Kara Sea	
	$\delta^{13}C$	CH_4	$\delta^{13}C$	CH_4	$\delta^{13}C$	CH_4	$\delta^{13}C$	CH_4
N of values	825	825	2372	2372	6114	6114	14,068	14,068
Min	−54.4	1.971	−53	1.952	−54.48	1.953	−54	1.953
Max	−45.4	2.096	−42.4	2.025	−41.4	2.189	−40.9	2.007
Mean	−49.49	2.005	−47.7	1.968	−47.81	1.962	−48.1	1.968
Median	−49.47	2.001	−47.8	1.973	−47.64	1.960	−48.18	1.967
1 quartile	−50.84	1.979	−49.1	1.955	−49.08	1.956	−49.5	1.964
3 quartile	−48.06	2.026	−46.3	1.978	−46.38	1.964	−46.7	1.970
St. deviation	1.78	0.028	1.87	0.012	2.02	0.012	1.85	0.007

Table 1. *Cont.*

29 July–25 August AMK-84	Port		White Sea		Barents Sea		Norwegian Sea	
	$\delta^{13}C$	CH_4	$\delta^{13}C$	CH_4	$\delta^{13}C$	CH_4	$\delta^{13}C$	CH_4
N of values	208	208	1500	1500	10,406	10,406	25,358	25,358
Min	−60.73	2.003	−50.39	1.979	−52.47	1.968	−56.28	1.946
Max	−43.21	6.054	−42.73	2.013	−42.63	2.054	−43.18	1.999
Mean	−46.97	2.069	−46.79	1.989	−47.44	1.980	−49.54	1.969
Median	−46.83	2.013	−46.79	1.986	−47.4	1.981	−49.41	1.969
1 quartile	−47.54	2.008	−47.50	1.984	−48.4	1.975	−51.08	1.963
3 quartile	−46.1	2.021	−46.06	1.993	−46.4	1.985	−47.92	1.973
St. deviation	1.97	0.423	1.1	0.007	1.47	0.006	2.12	0.01
27 August–29 September AMK-85	**Port**		**White Sea**		**Barents Sea**		**Kara Sea**	
	$\delta^{13}C$	CH_4	$\delta^{13}C$	CH_4	$\delta^{13}C$	CH_4	$\delta^{13}C$	CH_4
N of values	1645	1645	2460	2460	3598	3598	35,831	35,831
Min	−57.07	2.016	−54.07	1.958	−54.16	1.973	−55.59	1.966
Max	−47	2.845	−45.42	2.096	−45.08	2.063	−44.58	2.694
Mean	−51.03	2.155	−49.72	2.018	−49.83	2.008	−50.05	2.015
Median	−51.03	2.089	−49.75	2.005	−49.83	1.994	−50.07	2.012
1 quartile	−51.82	2.068	−50.79	1.981	−50.8	1.989	−50.95	2.002
3 quartile	−50.16	2.208	−48.64	2.06	−48.84	2.028	−49.18	2.026
St. deviation	1.28	0.128	1.52	0.039	1.42	0.027	1.31	0.022

During the AMK-83 cruise, the average CH_4 concentrations are recorded at the level of 1.962–1.968 ppm (Figure 4) for all seas, from the White to the Kara. The most intense emissions from wetlands are also noted during this period [42]. The lowest concentration of methane in the ambient air is observed in the Norwegian Sea (average 1.969 ppm) at the end of summer, in AMK-84. A gradual accumulation of methane in the ambient air begins in the Barents and White Seas, with average values reaching 1.980 and 1.989 ppm, respectively. The average methane concentration in all seas exceeded 2 ppm during the AMK-85 expedition, a significant part of which took place in September. During this period, there is already an active accumulation of methane in the Arctic and a weakening of the intensity of its sinks, while such a source as wetlands is no longer as significant as in the middle of summer [42]. Emissions become less significant, and methane sinks also become weaker as the temperature decreases [42]. This voyage is also interesting because of the greatest variety of directions of air masses advection.

Figure 4 shows the distribution functions of methane concentration for different seas, covered in the three analyzed expeditions. A rather small variation of CH_4 concentrations is typical for summer cruise, with a standard deviation of 0.007–0.01 for AMK-83 cruise and 0.006–0.01 for AMK-84 (Figure 3a–f, Table 1). A bimodal structure is distinguished in some cases, as, for example, for the White Sea in AMK-83 and AMK-85 (Figure 3a,g), which is a consequence of two dominant directions of air flow transport—from Scandinavia and from the northwest, without crossing land areas.

The concentration of methane is always higher in the port of Arkhangelsk, where many anthropogenic sources are permanently active, than those observed over the open seas. The maximum was noted during the September expedition; the average value reaches 2.155 ppm. Because of the significant anthropogenic burden, data of port of Arkhangelsk were not analyzed in the paper.

Trajectory analysis. The backward five-day trajectories (every 6 h for 00, 06, 12, 18 UTC) of air flows, built on the basis of the NOAA Hysplit Lagrangian transport model [43,44], were analyzed for all expeditions. To build trajectories, we used GDAS meteorology 1 × 1, model vertical velocity; the end point is 500 m above sea level. Series of methane concentration with generalized transport direction were constructed (Figure 5).

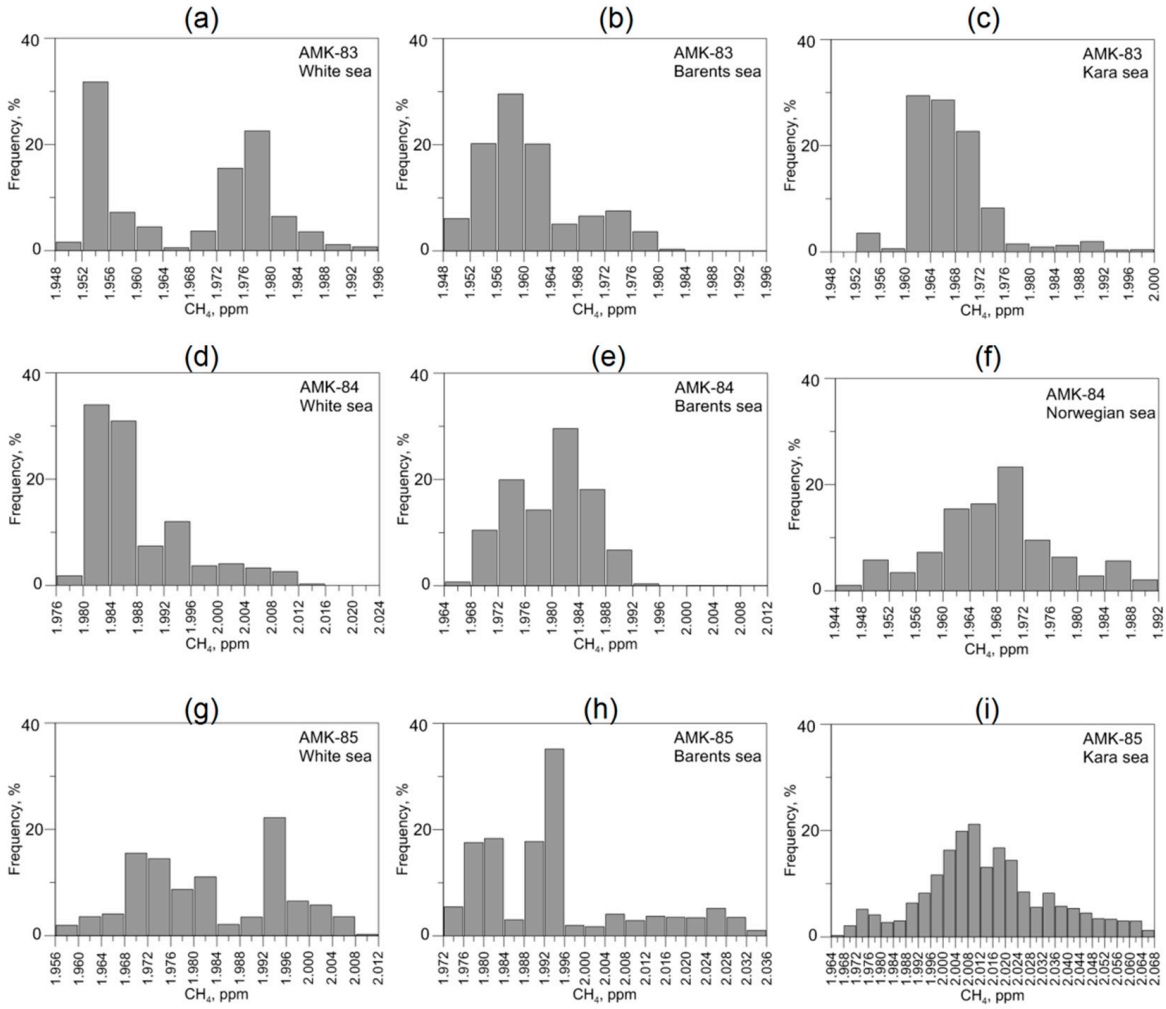

Figure 4. The frequency distribution of atmospheric CH_4 for different seas during AMK-83 (panels (**a**–**c**)), AMK-84 (panels (**d**–**f**)), and AMK-85 (panels (**g**–**i**)) (1-minute averaging data).

AMK-83 expedition was carried out during the period of low methane content in the surface air in late June–early July. The lower methane concentration corresponds to the advection from the southwest, from the North Atlantic, according to the trajectory analysis. On the AMK-83 cruise, the minimum methane concentration corresponds to the air flow from the Baltic, which was recorded once for the entire period on 19 June from 19:30 to 20:00 UTC and gives the averaged methane mole fraction as 1.954 ppm. Decreased values also correspond to the advection from the west and northwest, in cases where the flow did not cross the Scandinavian Peninsula (on average 1.956 ppm, in some cases 1.966 ppm). Correspondingly, an average of 1.977 ppm was noted when the air flow crossed Scandinavia, and the trajectories from Taimyr corresponded to a CH_4 content equal to an average of 1.970 ppm, which is a relatively high value.

During this period, no natural fires were recorded on the peninsula; in addition, a rather low methane abundance is noted at the Dikson ground station (Dikson island, Krasnoyarsk Region, Russia) during this time [45]. During the northern advection, the methane content above the sea surface was at the level of 1.966 ppm. The highest values of methane concentration in AMK-83 correspond to the removal from the east and southeast, from the Gydan Peninsula and Yamal, where some of the largest gas production and natural gas transportation regions in Russia are concentrated; the average CH_4 concentration was 1.988 ppm.

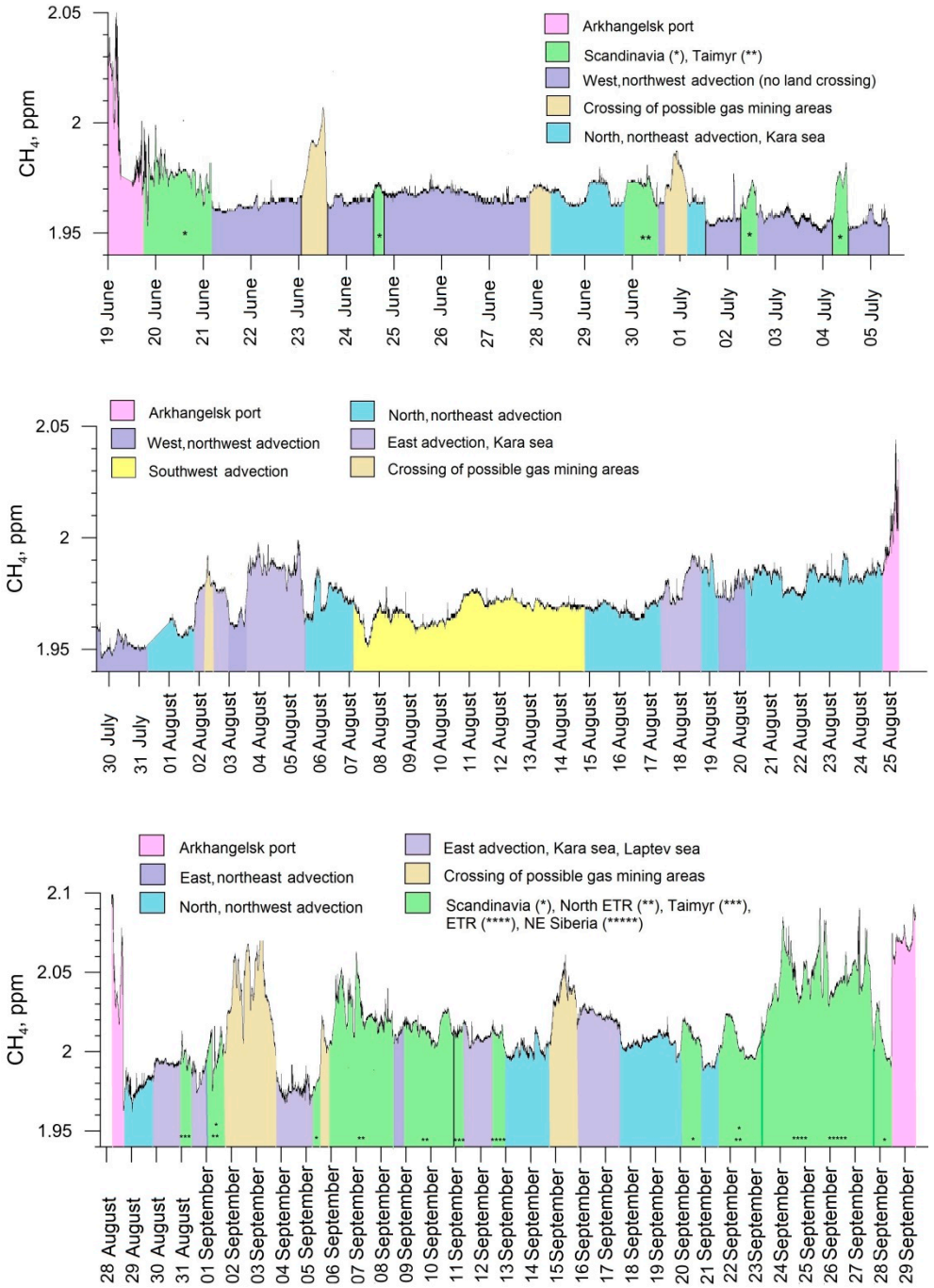

Figure 5. CH_4 mole fraction depending on direction of atmospheric flow for AMK-83, AMK-84, and AMK-85. The color indicates the geographic areas and the direction of transport according to the 120 h NOAA Hysplit backward trajectories. In some cases, the trajectory covered several regions; the corresponding asterisks (*) correspond to such periods on the graphs.

The same patterns are observed on the AMK-84 as on the previous one. The minimum methane concentration was noted in the Norwegian Sea on 30 and 31 July 2021. The average methane concentration was 1.952, with a minimum of 1.946 ppm for the northern and north-western transport (Table 1, Figure 5). The average methane concentration slightly increased to 1.959 ppm for a northern wind in the Norwegian Sea. Increased values of CH_4 concentration are noted during the eastern transport, on average 1.982 ppm. The average methane mole fraction reaches 1.969 ppm with the southwestern transport. The CH_4 content slightly increases in the Kara and White Seas, where, with north and northeastern

winds, the average value reaches 1.980 ppm, and, with north/northwestern outflow, the concentration increased to 1.981 ppm.

The longest cruise was AMK-85, the main part of which took place in September 2021, significantly repeating the route of AMK-83. The White and Barents Seas were covered for a significant part of the time (from 31.08 to 14.09) that the vessel spent in the Kara Sea, near the southwestern part of the Novaya Zemlya. This voyage exhibits the highest variability in methane concentration as well as the greatest variation in the direction of air flows. By September, a seasonal increase in the CH_4 content is also noticeable in the surface layer of the atmosphere. So, the minimum concentration of CH_4 is noted at the beginning of the expedition in the White Sea during the western air transfer from the Scandinavian Peninsula (average 1.972 ppm, minimum 1.958 ppm). In the Barents Sea, advection from the north and northeast prevailed. The average methane concentration was 1.978 ppm; the methane concentration slightly increased, up to 1.995 ppm, with air capture from Taimyr.

The ship spent a long time in the roadstead southeast of Novaya Zemlya in the Kara Sea. The increased methane concentration during this period corresponds to the advection from the mainland, especially from the gas production areas, where the CH_4 concentration significantly exceeds 2 ppm. A minimum of methane of 1.966 ppm is noted for the advection from the west in the Kara Sea. CH_4 is always above 2 ppm for the eastern directions of transport. The concentration rises sharply, up to 2.060 ppm, in the case of air flow crossing the mainland, especially regions of possible natural gas production. The increased methane concentration corresponds to the transport from the southern regions of Russian European territory and the north of Kazakhstan for the AMK-85 cruise (Figure 4, 24–27 September 2021, the average methane concentration is 2.050 ppm). Anthropogenic sources and natural fires are considered as possible reasons for the increased concentration of methane, which still took place in the European Territory of Russia and the Urals.

Isotopic composition. Figure 6 shows the $\delta^{13}C$ variability. In all likelihood, the ships almost all of the time were distant from methane sources.

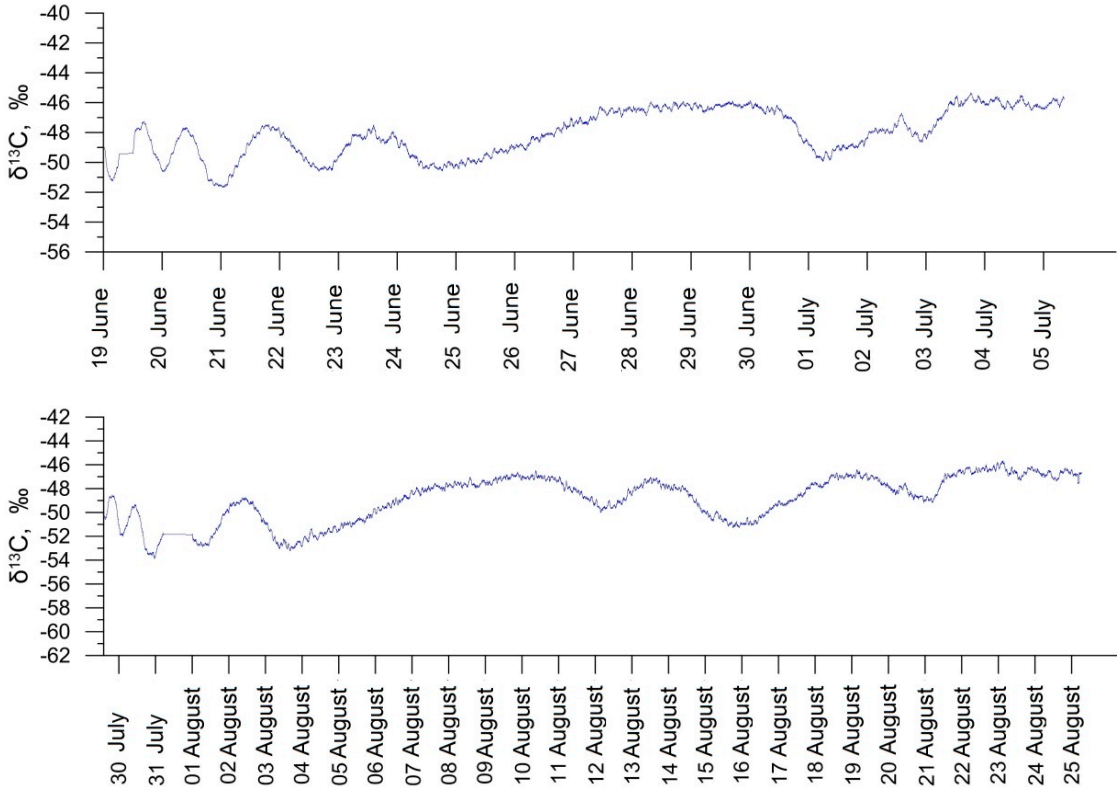

Figure 6. *Cont.*

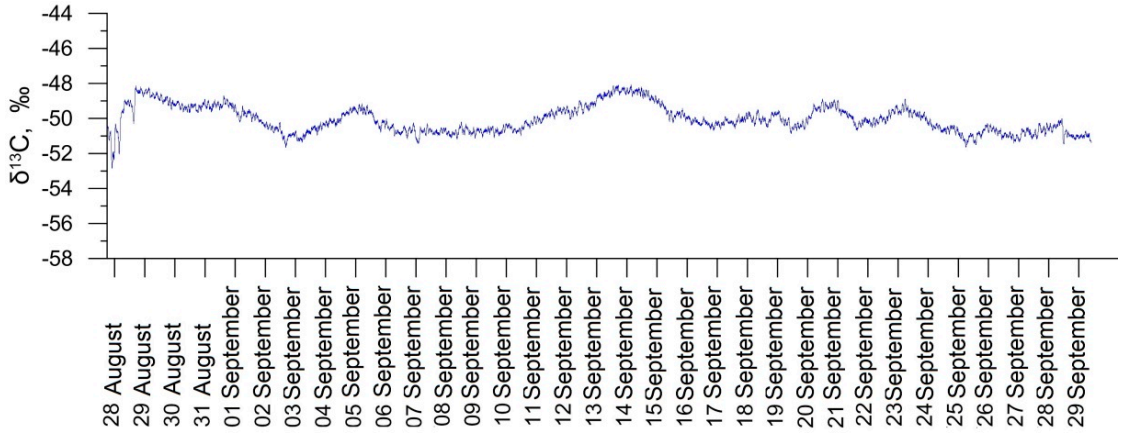

Figure 6. $\delta^{13}C$ variability during AMK-83, AMK-84, and AMK-85 (1 h averaging).

The Keeling plot method was used for more accurate analysis of potential methane contributors [46–48]. The largest possible range of mixing ratios of CH_4 in the air mass is required to ensure maximum accuracy in determining the isotopic characterization of excess methane in the air mass. The difficulty in identifying sources during ship-borne measurements is that the air flow is not uniform and accumulates methane from several sources while passing over different areas. Figure 7 shows examples of Keeling plots.

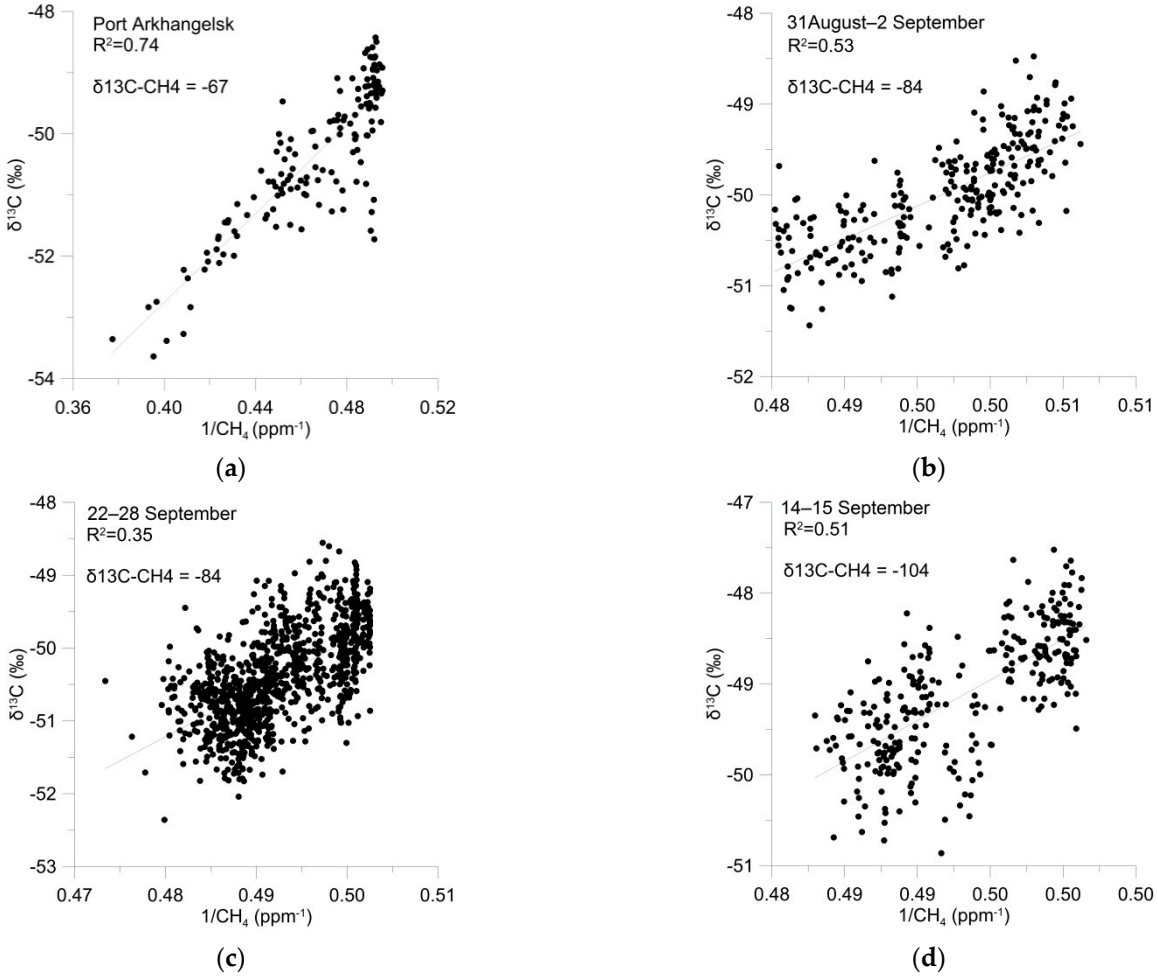

Figure 7. Keeling plot for some areas of AMK-85 (10 min averaging). (**a**) dominance of emissions from wetlands, the port of Arhangelsk. First line for panels (**b**–**d**)—date (dd.mm).

Despite a significant anthropogenic burden around the port of Arkhangelsk, the Keeling plot shows dominance of emissions from wetlands (Figure 7a). Figure 7b,c show that values are outside the range (more depleted) than expected for Finland wetlands [32]. But this range of values was typical for this investigation. Figure 7b,c are well outside the range (more depleted) than expected for northern wetlands. Figure 7d is much more depleted than expected wetland sources. It is within the range of $d^{13}C$ reported for ESAS sediment sources in [34]. So, a seafloor source of CH_4 is possibly represented here. The results are consistent with data published, for example, in [40], where it was shown that at the Nordic Seas the share of methane emissions from hydrates dominates.

4. Discussion and Conclusions

Observations of both methane concentration and its isotopic ratio $\delta^{13}C$ were carried out in summer and autumn of 2021 in the Arctic aboard the R/V Akademik Mstislav Keldysh. As expected, during the period covered by the research, a significant influence on the methane concentration variability in the lower atmosphere is determined mainly by large-scale processes, namely by the direction of air masses advection. The minimum methane concentration during the expeditions occurred in Arctic spring and summer, observed due to air mass removal from the west direction. A similar result was obtained, for example, during a marine expedition [40] where the minimum was obtained in the western seas of the Arctic. The maximum methane concentration in the ambient air is observed during advection from the northwest of Siberia (areas of potential natural gas production and transportation). In the autumn period, the highest methane concentration was recorded during advection from natural gas production areas (northwest of Siberia) and invasion from the south of the European territory of Russia and north of Kazakhstan, where the anthropogenic load was high and wildfires were noted (https://firms.modaps.eosdis.nasa.gov/map/, last accessed on 20 December 2021). However, the ship, almost all of the time, was at a considerable distance from methane sources. The Keeling plot analysis did not reveal a prevailing source of methane during all three campaigns. According to the analysis, results emissions from freshwater sources, wetlands, seafloor sources, and hydrates contribute to the measured variations.

Author Contributions: All authors contributed to the original draft preparation of the manuscript; I.B. and V.B. conceived and designed the experiments; V.M. took part in expeditions and collected data; N.P. contributed to the data analysis; A.S. and M.F. provided projects administration and revised the whole manuscript. All authors have read and agreed to the published version of the manuscript.

Funding: This work was funded by the Russian Science Foundation under grant №20-17-00200 (observations) and by the grant N 075-15-2021-934 in the form of a subsidy from Ministry of Science and Higher Education of Russia, Moscow, Russia (data interpretation). Field research was supported by the state assignment, no. 0128-2021-007/.

Acknowledgments: We thank our ship crew of Shirshov Institute of Oceanology RAS (Moscow, Russia) for supporting and help in gathering datasets. The authors gratefully acknowledge M. Kravchishina and E. Dubinina for supervising of oceanographic campaigns.

Conflicts of Interest: The authors declare no conflict of interest.

References

1. Kirschke, S.; Bousquet, P.; Ciais, P.; Saunois, M.; Canadell, J.G.; Dlugokencky, E.J.; Bergamaschi, P.; Bergmann, D.; Blake, D.R.; Bruhwiler, L.; et al. Three decades of global methane sources and sinks. *Nat. Geosci.* **2013**, *6*, 813–823. [CrossRef]
2. Saunois, M.; Bousquet, P.; Poulter, B.; Peregon, A.; Ciais, P.; Canadell, J.G.; Dlugokencky, E.J.; Etiope, G.; Bastviken, D.; Houweling, S.; et al. The global methane budget 2000–2012. Earth. *Syst. Sci. Data* **2016**, *8*, 697–751. [CrossRef]
3. Saunois, M.; Stavert, A.R.; Poulter, B.; Bousquet, P.; Canadell, J.G.; Jackson, R.B.; Raymond, P.A.; Dlugokencky, E.J.; Houweling, S.; Patra, P.K.; et al. The global methane budget 2000–2017. *Earth Syst. Sci. Data* **2020**, *12*, 1561–1623. [CrossRef]
4. Shakhova, N.N.; Semiletov, I.I.; Salyuk, A.A.; Yusupov, V.V.; Kosmach, D.D.; Gustafsson, Ö.Ö. Extensive methane venting to the atmosphere from sediments of the East Siberian Arctic Shelf. *Science* **2010**, *327*, 1246–1250. [CrossRef] [PubMed]

5. Shakhova, N.; Semiletov, I.; Leifer, I.; Sergienko, V.; Salyuk, A.; Kosmach, D.; Chernykh, D.; Stubbs, C.; Nicolsky, D.; Tumskoy, V.; et al. Ebullition and storm-induced methane release from the East Siberian Arctic Shelf. *Nat. Geosci.* **2014**, *7*, 64–70. [CrossRef]
6. Yurganov, L.; Carroll, D.; Zhang, H. Ocean stratification and sea-ice cover in Barents and Kara seas modulate sea-air methane flux: Satellite evidence. *Earth Space Sci.* **2020**, *18*, 118–140.
7. Fenwick, L.; Capelle, D.; Damm, E.; Zimmermann, S.; Williams, W.J.; Vagle, S.; Tortell, P. Methane and nitrous oxide distributions across the North American Arctic Ocean during summer, 2015. *J. Geophys. Res. Oceans* **2017**, *122*, 390–412. [CrossRef]
8. Thornton, B.F.; Prytherch, J.; Andersson, K.; Brooks, I.M.; Salisbury, D.; Tjernström, M.; Crill, P.M. Shipborne eddy covariance observations of methane fluxes constrain Arctic sea emissions. *Sci. Adv.* **2020**, *6*, 7934. [CrossRef]
9. Pankratova, N.; Skorokhod, A.; Belikov, I.; Elansky, N.; Rakitin, V.; Shtabkin, Y.; Berezina, E. Evidence of atmospheric response to methane emissions from the east siberian arctic shelf. *Geogr. Environ. Sustain.* **2018**, *11*, 85–92. [CrossRef]
10. Skorokhod, A.I.; Pankratova, N.V.; Belikov, I.B.; Thompson, R.L.; Novigatsky, A.N.; Golitsyn, G.S. Observations of atmospheric methane and its stable isotope ratio (δ^{13}C) over the Russian Arctic seas from ship cruises in the summer and autumn of 2015. *Dokl. Earth Sci.* **2016**, *470*, 1081–1085. [CrossRef]
11. Pankratova, N.V.; Belikov, I.B.; Belousov, V.A.; Kopeikin, V.M.; Skorokhod, A.I.; Shtabkin, Y.A.; Malafeev, G.V.; Flint, M.V. Concentration and Isotopic Composition of Methane, Associated Gases, and Black Carbon over Russian Arctic Seas (Shipborne Measurements). *Oceanology* **2020**, *60*, 593–602. [CrossRef]
12. Shakhova, N.; Semiletov, I.; Chuvilin, E. Understanding the Permafrost–Hydrate System and Associated Methane Releases in the East Siberian Arctic Shelf. *Geosciences* **2019**, *9*, 251. [CrossRef]
13. Bogoyavlensky, V.; Kishankov, A.; Yanchevskaya, A.; Bogoyavlensky, I. Forecast of Gas Hydrates Distribution Zones in the Arctic Ocean and Adjacent Offshore Areas. *Geosciences* **2018**, *8*, 453. [CrossRef]
14. Archer, D. A model of the methane cycle, permafrost, and hydrology of the Siberian continental margin. *Biogeosciences* **2015**, *12*, 2953–2974. [CrossRef]
15. Wåhlström, I.; Dieterich, C.; Pemberton, P.; Meier, H.E.M. Impact of increasing inflow of warm Atlantic water on the sea-air exchange of carbon dioxide and methane in the Laptev Sea. *J. Geophys. Res. Biogeosciences* **2016**, *121*, 1867–1883. [CrossRef]
16. Berchet, A.; Pison, I.; Chevallier, F.; Paris, J.-D.; Bousquet, P.; Bonne, J.-L.; Arshinov, M.Y.; Belan, B.D.; Cressot, C.; Davydov, D.K.; et al. Natural and anthropogenic methane fluxes in Eurasia: A mesoscale quantification by generalized atmospheric inversion. *Biogeosciences* **2015**, *12*, 5393–5414. [CrossRef]
17. Tohjima, Y.; Zeng, J.; Shirai, T.; Niwa, Y.; Ishidoya, S.; Taketani, F.; Sasano, D.; Kosugi, N.; Kameyama, S.; Takashima, H.; et al. Estimation of CH4 emissions from the East Siberian Arctic Shelf based on atmospheric observations aboard the R/V Mirai during fall cruises from 2012 to 2017. *Polar Sci.* **2021**, *27*, 100571. [CrossRef]
18. Yurganov, L.N.; Leifer, I. Estimates of methane emission rates from some Arctic and sub-Arctic areas, based on orbital interferometer IASI data. *Sovrem. Probl. Distancionnogo Zondirovaniya Zemli Iz Kosm.* **2016**, *13*, 173–183. [CrossRef]
19. Jackson, R.; Saunois, M.; Bousquet, P.; Canadell, J.G.; Poulter, B.; Stavert, A.; Bergamaschi, P.; Niwa, Y.; Segers, A.; Tsuruta, A. Increasing anthropogenic methane emissions arise equally from agricultural and fossil fuel sources. *Environ. Res. Lett.* **2020**, *15*, 071002. [CrossRef]
20. Thornton, B.F.; Wik, M.; Crill, P.M. Double-counting challenges the accuracy of high-latitude methane inventories. *Geophys. Res. Lett.* **2016**, *43*, 12569–12577. [CrossRef]
21. Myhre, C.L.; Ferre, B.; Platt, S.M.; Silyakova, A.; Hermansen, O.; Allen, G.; Pisso, I.; Schmidbauer, N.; Stohl, A.; Pitt, J.; et al. Extensive release of methane from Arctic seabed west of Svalbard during summer 2014 does not influence the atmosphere. *Geophys. Res. Lett.* **2016**, *43*, 4624–4631. [CrossRef]
22. Schuur, E.A.G.; Vogel, J.G.; Crummer, K.G.; Lee, H.; Sickman, J.O.; Osterkamp, T.E. The effect of permafrost thaw on old carbon release and net carbon exchange from tundra. *Nature* **2009**, *459*, 556–559. [CrossRef]
23. Anthony, K.M.W.; Anthony, P.; Grosse, G.; Chanton, J.P. Geologic methane seeps along boundaries of Arctic permafrost thaw and melting glaciers. *Nat. Geosci.* **2012**, *5*, 419–426. [CrossRef]
24. Kort, E.A.; Wofsy, S.C.; Daube, B.C.; Diao, M.; Elkins, J.W.; Gao, R.S.; Hintsa, E.J.; Hurst, D.F.; Jimenez, R.; Moore, F.L.; et al. Atmospheric observations of Arctic Ocean methane emissions up to 82° north. *Nat. Geosci.* **2012**, *5*, 318–321. [CrossRef]
25. Zhang, F.; Zhang, H.; Pei, S.; Zhan, L.; Ye, W. Effects of Arctic Warming on Microbes and Methane in Different Land Types in Svalbard. *Water* **2021**, *13*, 3296. [CrossRef]
26. Olefeldt, D.; Turetsky, M.R.P.; Crill, M.; McGuire, A.D. Environmental and physical controls on northern terrestrial methane emissions across permafrost zones. *Glob. Chang. Biol.* **2012**, *19*, 589–603. [CrossRef]
27. Bloom, A.A.; Palmer, P.I.; Fraser, A.; Reay, D.S.; Frankenberg, C. Large-scale controls of methanogenesis inferred from methane and gravity spaceborne data. *Science* **2010**, *327*, 322–325. [CrossRef]
28. McGuire, A.D.; Anderson, L.G.; Christensen, T.R.; Dallimore, S.; Guo, L.; Hayes, D.J.; Heimann, M.; Lorenson, T.D.; Macdonald, R.W.; Roulet, N. Sensitivity of the carbon cycle in the Arctic to climate change. *Ecol. Monogr.* **2009**, *79*, 523–555. [CrossRef]
29. Berchet, A.; Bousquet, P.; Pison, I.; Locatelli, R.; Chevallier, F.; Paris, J.-D.; Dlugokencky, E.J.; Laurila, T.; Hatakka, J.; Viisanen, Y.; et al. Atmospheric constraints on the methane emissions from the East Siberian Shelf, Atmos. *Chem. Phys.* **2016**, *16*, 4147–4157. [CrossRef]

30. Bousquet, P.; Ciais, P.; Miller, J.B.; Dlugokencky, E.J.; Hauglustaine, D.A.; Prigent, C.; Van der Werf, G.R.; Peylin, P.; Brunke, E.G.; Carouge, C.; et al. Contribution of anthropogenic and natural sources to atmospheric methane variability. *Nature* **2016**, *443*, 439–443. [CrossRef]
31. Fisher, R.E.; Sriskantharajah, S.; Lowry, D.; Lanoisellé, M.; Fowler, C.M.R.; James, R.H.; Hermansen, O.; Myhre, C.L.; Stohl, A.; Greinert, J.; et al. Arctic methane sources: Isotopic evidence for atmospheric inputs. *Geophys. Res. Lett.* **2011**, *38*, L21803. [CrossRef]
32. Levin, I.; Veidt, C.; Vaughn, B.H.; Brailsford, G.; Bromley, T.; Heinz, R.; Lowe, D.; Miller, J.B.; Poss, C.; White, J.W.C. No inter-hemispheric delta (CH4)-C-13 trend observed. *Nature* **2012**, *486*, E3–E4. [CrossRef]
33. Fisher, R.E.; France, J.L.; Lowry, D.; Lanoisellé, M.; Brownlow, R.; Pyle, J.A.; Cain, M.; Warwick, N.; Skiba, U.M.; Drewer, J.; et al. Measurement of the ^{13}C isotopic signature of methane emissions from northern European wetlands. *Glob. Biogeochem. Cycles* **2017**, *31*, 605–623. [CrossRef]
34. Gupta, M.; Tyler, S.; Cicerone, R. Modeling atmospheric $^{13}CH_4$ and the causes of recent changes in atmospheric CH4 amounts. *J. Geophys. Res.* **1996**, *101*, 22923–22932. [CrossRef]
35. Dlugokencky, E.J.; Nisbet, E.G.; Fisher, R.; Lowry, D. Global atmospheric methane: Budget, changes and dangers. *Philos. Trans. R. Soc. A* **2011**, *369*, 2058–2072. [CrossRef]
36. Sapart, C.J.; Shakhova, N.; Semiletov, I.; Jansen, J.; Szidat, S.; Kosmach, D.; Dudarev, O.; van der Veen, C.; Egger, M.; Sergienko, V.; et al. The origin of methane in the East Siberian Arctic Shelf unraveled with triple isotope analysis. *Biogeosciences* **2017**, *14*, 2283–2292. [CrossRef]
37. Sherwood, O.A.; Schwietzke, S.; Arling, V.A.; Etiope, G. Global Inventory of Gas Geochemistry Data from Fossil Fuel, Microbial and Burning Sources, version 2017. *Earth Syst. Sci. Data* **2017**, *9*, 639–656. [CrossRef]
38. Berchet, A.; Pison, I.; Crill, P.M.; Thornton, B.; Bousquet, P.; Thonat, T.; Hocking, T.; Thanwerdas, J.; Paris, J.-D.; Saunois, M. Using ship-borne observations of methane isotopic ratio in the Arctic Ocean to understand methane sources in the Arctic. *Atmos. Chem. Phys.* **2020**, *20*, 3987–3998. [CrossRef]
39. Pisso, I.; Myhre, C.L.; Platt, S.M.; Eckhardt, S.; Hermansen, O.; Schmidbauer, N.; Mienert, J.; Vadakkepuliyambatta, S.; Bauguitte, S.; Pitt, J.; et al. Constraints on oceanic methane emissions west of Svalbard from atmospheric in situ measurements and Lagrangian transport modeling. *J. Geophys. Res.-Atmos.* **2016**, *121*, 025590. [CrossRef]
40. Yu, J.; Xie, Z.; Sun, L.; Kang, H.; He, P.; Xing, G. $\delta^{13}C$-CH_4 reveals CH_4 variations over oceans from mid-latitudes to the Arctic. *Sci. Rep.* **2015**, *5*, 13760. [CrossRef]
41. France, J.L.; Cain, M.; Fisher, R.E.; Lowry, D.; Allen, G.; O'Shea, S.J.; Illingworth, S.; Pyle, J.; Warwick, N.; Jones, B.T.; et al. Measurements of $\delta^{13}C$ in CH_4 and using particle dispersion modeling to characterize sources of Arctic methane within an air mass. *J. Geophys. Res. Atmos.* **2016**, *121*, 14257–14270. [CrossRef] [PubMed]
42. Warwick, N.J.; Cain, M.L.; Fisher, R.; France, J.L.; Lowry, D.; Michel, S.E.; Nisbet, E.G.; Vaughn, B.H.; White, J.W.C.; Pyle, J.A. Using $\delta^{13}C$-CH_4 and δD-CH_4 to constrain Arctic methane emissions. *Atmos. Chem. Phys.* **2016**, *16*, 14891–14908. [CrossRef]
43. Stein, A.F.; Draxler, R.R.; Rolph, G.D.; Stunder, B.J.B.; Cohen, M.D.; Ngan, F. NOAA's HYSPLIT atmospheric transport and dispersion modeling system. *Bull. Amer. Meteor. Soc.* **2015**, *96*, 2059–2077. [CrossRef]
44. Rolph, G.; Stein, A.; Stunder, B. Real-time Environmental Applications and Display sYstem: READY. *Environ. Model. Softw.* **2017**, *95*, 210–228. [CrossRef]
45. Panov, A.; Prokushkin, A.; Kübler, K.R.; Korets, M.; Urban, A.; Bondar, M.; Heimann, M. Continuous CO_2 and CH_4 Observations in the Coastal Arctic Atmosphere of the Western Taimyr Peninsula, Siberia: The First Results from a New Measurement Station in Dikson. *Atmosphere* **2021**, *12*, 876. [CrossRef]
46. Keeling, C.D. The concentration and isotopic abundances of atmospheric carbon dioxide in rural areas. *Geochim. Cosmochim. Acta* **1958**, *13*, 322–334. [CrossRef]
47. Pataki, D.E.; Ehleringer, J.R.; Flanagan, L.B.; Yakir, D.; Bowling, D.R.; Still, C.J.; Buchmann, N.; Kaplan, J.O.; Berry, J.A. The application and interpretation of Keeling plots in terrestrial carbon cycle research. *Glob. Biogeochem. Cycles* **2003**, *17*, 1022. [CrossRef]
48. Sriskantharajah, S.; Fisher, R.E.; Lowry, D.; Aalto, T.; Hatakka, J.; Aurela, M.; Laurila, T.; Lohila, A.; Kuitunen, E.; Nisbet, E.G. Stable carbon isotope signatures of methane from a Finnish subarctic wetland. *Tellus Ser. B* **2012**, *64*, 18818. [CrossRef]